Three-Dimensional Reconstruction of Native and Reassembled *Lumbricus terrestris* Extracellular Hemoglobin. Localization of the Monomeric Globin Chains[†]

Felix de Haas,[‡,§] Askar Kuchumov,[||] Jean-Christophe Taveau,[‡] Nicolas Boisset,[‡] Serge N. Vinogradov,[||] and Jean N. Lamy*[,‡]

Laboratoire de Biochimie Fondamentale and URA 1334 CNRS, 2 bis Boulevard Tonnellé, F-37032 Tours Cedex, France, and Department of Biochemistry, Wayne State University School of Medicine, Detroit, Michigan 48201

Received January 22, 1997; Revised Manuscript Received April 7, 1997[⊗]

ABSTRACT: The ∼3.5 MDa hexagonal bilayer (HBL) hemoglobin (Hb) of the earthworm *Lumbricus terrestris* is composed of monomers and disulfide-bonded trimers (T) of globin chains and of four types of heme-deficient linker chains (L). Cryoelectron microscopic images of native Hb and of HBL reassembled from the constituent subunits depleted in monomer subunit (HBL[T+L]) were subjected to three-dimensional reconstructions by the random conical tilt series method. Native Hb has an architecture very similar to those of other annelid and vestimentiferan Hbs, consisting of 12 hollow globular substructures (HGS). Each HGS is comprised of six dense masses, has a 3-fold symmetry, and is organized in two hexagonally symmetric layers, with the vertices of the upper layer rotated 16° clockwise relative to those of the lower layer. The layers are tethered to a central linker complex, consisting of two bracelets of connections perpendicular to the 6-fold axis and a set of six vertical connections linked to a flat hexagonal mass. HBL[T+L] shared all these features with the native Hb, except for a large hole around the 3-fold symmetry axis in each HGS, indicating the probable location of the missing monomer subunit.

The ∼3.5 MDa extracellular hemoglobins (Hb) of annelids and vestimentiferans are large hexagonal bilayer (HBL) complexes of globin and nonglobin chains, with a characteristic, hexagonally symmetric bilayer appearance in electron micrographs (Lamy *et al*., 1996). A "bracelet" model of the quaternary structure of a prototype HBL Hb, namely that of the earthworm *Lumbricus terrestris*, was proposed to consist of 12 complexes of globin subunits, each comprised of a disulfide-bonded trimer subunit (chains a + b + c, ∼53 kDa) and a monomer subunit (chain d, ∼17 kDa), tethered to a central complex of nonglobin linker chains which form four groups ranging in mass from 24 to 32 kDa (Vinogradov *et al*., 1986). The 12 complexes of globin chains were found to be dodecamers of chains a−d, $[a + b + c]_3[d]_3$ (Vinogradov *et al*., 1991), and recent electrospray ionization mass spectrometry (ESI-MS), scanning transmission electron microscopy (STEM) mass mapping, and sedimentation equilibrium studies indicate that 36 or 42 linker chains form the central complex in agreement with an overall mass of 3.66 MDa (Martin *et al*., 1996b). Riggs and his collaborators have proposed that the 12 globin complexes are hexadecamers of the four globin chains, $[a + b + c]_4[d]_4$ and that they are held together by only 24 linker chains, corresponding to a much higher overall mass of ∼4.1 MDa (Ownby *et al*., 1993, Zhu *et al*., 1996a,b). The D_6 point-group symmetry observed for crystals and electron microscopic (EM) images of *Lumbricus* Hb (Royer *et al*., 1987; Royer & Hendrickson, 1988; Boekema & Van Heel, 1989) and three-dimensional (3D) reconstructions from EM images of two-dimensional crystals of other annelid Hbs (Cejka *et al*., 1989, 1991, 1992) was verified by the first 3D reconstruction of *Lumbricus* Hb in vitreous ice by cryoelectron microscopy (Schatz *et al*., 1995). Furthermore, this study showed that each of the 12 substructures has a local 3-fold axis of symmetry. This is in agreement with the symmetry found for the dodecamer subunit crystals (Martin *et al*., 1996a) and was expected on the basis of its M_3T_3 structure (Vinogradov *et al*., 1991). More recent 3D reconstructions carried out by the random conical tilt series method on cryoelectron microscopic images of the chlorocruorin (Chl) from the marine polychaete *Eudistylia* (De Haas *et al*., 1996b) and the Hb from the leech *Macrobdella* (De Haas *et al*., 1996a) suggest that annelid HBL Hbs have similar quaternary structures. In addition, the results obtained with Hbs from the vestimentiferan *Riftia* (De Haas *et al*., 1996c) and the polychaete *Alvinella* (De Haas *et al*., 1996d), which inhabit the sulfide-rich hydrothermal vents at 2500 m on the Pacific Ocean floor (Lamy *et al*., 1996), demonstrate that all the foregoing HBL Hbs share the same structural features: (i) two layers of six hollow globular substructures (HGSs) and D_6 point-group symmetry; (ii) each HGS comprised of six dense masses related through a local 3-fold symmetry axis; and (iii) a linker complex, which consists of a flat central hexagonal mass and several bracelets of connections to the two HGS layers. Except for *Alvinella* Hb, the vertices of top hexagonal layer

[†] This research was supported in part by NIH Grant DK38674.

* To whom correspondence should be addressed. Tel: (33) 2 47 37 66 84. Fax: (33) 2 47 36 61 29. E-mail: lamy@univ-tours.fr.

[‡] Laboratoire de Biochimie Fondamentale and URA 1334 CNRS.

[§] Present address: European Molecular Biology Laboratory, Meyerhofstrasse1, D-69012 Heidelberg, Germany.

[||] Wayne State University School of Medicine.

[⊗] Abstract published in *Advance ACS Abstracts,* May 15, 1997.

[1] Abbreviations. Hb, hemoglobin; HBL, hexagonal bilayer; ESI-MS, electrospray ionization mass spectrometry; STEM, scanning transmission electron microscopy; EM, electron microscopy; 3D, three-dimensional; Chl, chlorocruorin; HGS, hollow globular substructure; HBL[T+L], HBL structure reassembled from trimers of globin chains and all the linker chains; SDS−PAGE, sodium dodecyl sulfate−polyacrylamide gel electrophoresis; RP-HPLC, reversed phase high-pressure liquid chromatography; DPR, differential phase residual; FSC, Fourier shell correlation.

S0006-2960(97)00131-1 CCC: $14.00

are rotated 16° clockwise relative to those of the bottom layer.

Studies of the reassembly of the HBL structure of *Lumbricus* Hb using STEM (Kapp *et al*., 1984) showed that it could also be obtained from the trimer and linker subunits only (Kapp *et al*., 1987), which is termed HBL[T+L]. In the present communication, we report a comparison of the 3D reconstructions of *Lumbricus* Hb and HBL[T+L], with the aims of determining the structural similarity between native and reassembled HBL structures as well as the locus of the monomer subunit within them.

EXPERIMENTAL PROCEDURES

Materials. *L. terrestris* Hb was prepared as described previously (Vinogradov *et al*., 1986; Vinogradov & Sharma, 1994). Following the complete dissociation of the Hb at alkaline pH (Kapp *et al*., 1987) or at neutral pH in the presence of 4 M urea (Sharma *et al*., 1996), peaks T+L and M were isolated by gel filtration and HBL[T+L] was reassembled in 0.1 M Tris-HCl buffer, 10 mM $CaCl_2$. The subunit compositions were assessed using sodium dodecyl sulfate−polyacrylamide gel electrophoresis (SDS−PAGE), reversed phase HPLC (RP-HPLC), and ESI-MS.

Analytical Methods. SDS−PAGE was carried out using 15% polyacrylamide slab gels (Laemmli, 1970) and staining with Coomassie Brillant Blue R250. The band densities were measured with a IS-1000 Digital Imaging System (Alpha Innotech Corp., San Leandro, CA 94577). RP-HPLC was performed with a 4.6 × 25 mm Synchropack RP C_{18} column (SynChrom, Inc., Lafayette, IN 47903), using an Isco model 2350 solvent delivery system (Isco, Inc., Lincoln, NE 68504). Protein was eluted with a 30−55% aqueous acetonitrile/0.1% TFA gradient in 90 min at a flow rate of 1 mL/min, and absorbance was monitored at 220 nm. ESI mass spectra of proteins in 50% aqueous acetonitrile/0.2% formic acid were acquired with a VG Quattro II electrospray ionization mass spectrometer (Micromass UK Ltd., Altrincham, Cheshire WA14 5RZ, U.K.) using maximum entropy processing (Martin *et al*., 1996b).

Cryoelectron Microscopy. To prevent aggregation of the molecules on the sample grid, 0.1 mg/mL dilutions of Hb and HBL[T+L] were prepared in 0.1 M Tris-HCl, buffer pH 7.2, 10 mM $CaCl_2$, 10 mM $MgCl_2$. Approximately 5 μL of the dilution were applied onto a 300 mesh copper grid coated with a holey carbon film. After blotting excess solution, the grid was rapidly plunged into liquid ethane (Dubochet *et al*., 1982; Adrian *et al*., 1984; Milligan *et al*., 1984). The specimen was loaded into a Philips CM12 electron microscope using a Gatan 626 cryotransfer system. The microscope was equipped with a Gatan CCD camera and a Gatan 651N anticontaminator maintained at −175 °C and examined at an accelerating voltage of 100 kV and a magnification of ×33910 for native Hb and ×34430 for HBL[T+L]. The magnification was determined from the diffraction pattern of a catalase crystal (Misell, 1978). Micrographs were recorded with minimal dose on Kodak SO 163 films and developed in full-strength Kodak D19 developer for 12 min.

For the calculation of the reference volume, images of native Hb were collected as follows. Each specimen field was recorded twice, with the grid respectively tilted at 45 and 0°. Pairs of micrographs were recorded at −2.7 μm defocus for both tilted-specimen and untilted-specimen fields. Due to the tilt angle of 45°, the value of −2.7 μm corresponds to a mean defocus of the tilted-specimen micrograph. Because of the gradient of defocus, the 3D reconstruction volume was not subjected to a correction of contrast transfer function. For the refined volumes of native Hb and HBL[T+L], the images were extracted from micrographs of the untilted-specimen recorded at −1.5 μm defocus. Both tilted- and untilted-specimen images of Hb and HBL[T+L] received an electron dose of 9 electrons/Å^2 assessed by the conversion efficiency of the CCD camera.

Image Processing

Digitization and Windowing. Micrographs were digitized with an Optronix P1000 drum microdensitometer using a square aperture and a scan step of 25 μm. This corresponds to a pixel size of 0.737 × 0.737 and 0.726 × 0.726 nm in the specimen of native Hb and HBL[T+L], respectively. For native Hb, the pairs of particles were windowed from the tilted- and untilted-specimen micrographs using an interactive selection program. The tilt angle and direction of the tilt axis were calculated at this step from the particle coordinates (Radermacher, 1988). For HBL[T+L], only untilted-specimen micrographs were used. All selected particles coded as arrays of optical densities were windowed, contrast inverted, and normalized so that their noise statistics would match a reference distribution corresponding to a portion of the micrograph free of particles and artifacts (Boisset *et al*., 1993). All programs used for image processing are part of the SPIDER (Frank *et al*., 1996) and SIGMA (Taveau, 1996) software packages.

3D Reconstruction. The 3D reconstruction of the reference volume of native Hb was carried out using a modification (Penczek *et al*., 1992, 1994) of the method of random conical tilt series (Radermacher *et al*., 1987a,b). The complete set of untilted-specimen images was first subjected to reference-free 2D alignment and sorted into homogeneous image classes by correspondence analysis (Van Heel & Frank, 1981) and hierarchical ascendant classification (Van Heel, 1984) using the Ward's merging criterion (Ward, 1963, Lebart *et al*., 1984). Then, the tilted-specimen images corresponding to the top and side views were subjected to 3D reconstruction, using the Simultaneous Iterative Reconstruction Technique (SIRT) (Gilbert *et al*., 1972) as proposed for EM images by Penczek *et al*. (1992). To reach an isotropic resolution, the corresponding primary 3D reconstruction volumes were aligned in a common orientation with the method of direct search in real space (Penczek *et al*., 1992). Rather than adding the primary volumes, a merged 3D reconstruction was processed from the selected original classes of tilted-specimen images after correcting their assigned Eulerian angles. Finally, the merged 3D reconstruction volume was refined with several cycles of 3D projection alignment (Penczek *et al*., 1994, Harauz & Ottensmeyer, 1984). At this stage, tilted-specimen images, which were initially disregarded because of their low frequency occurrence or their atypical overall shapes (intermediate views), were included in the image set and Eulerian angles were assigned to all the images by one cycle of 3D projection alignment. Then, for each projection direction defined by the first two Eulerian angles, ϕ and θ, the two images having the best correlation coefficient with the projection of the reference 3D volume were selected and a

3D reconstruction was carried out. Finally, the 3D reconstruction volume was refined with several cycles of 3D projection alignment. This volume is further designated as V_A.

For the refined volumes of native Hb and HBL[T+L], Eulerian angles were assigned by one cycle of 3D projection alignment using V_A as a reference to all the untilted-specimen images recorded at −1.5 μm defocus. Then, for each projection direction the two images having the best correlation coefficient were selected and a 3D reconstruction was carried out. Finally, the 3D reconstruction volume was refined with several cycles of 3D projection alignment.

Symmetry. The 6-fold rotational symmetry visible in the individual images in the top-view orientation suggests that, as for other HBL Hbs, *Lumbricus* Hb has a D_6 point-group symmetry (Royer *et al*., 1987; Boekema *et al*., 1989). The presence of an authentic D_6 point-group symmetry was checked by a previously described test based on the correlation coefficients between the 3D volume in its original position and after rotations around its 2-fold and 6-fold axes (Lambert *et al*., 1995). To take advantage of this symmetry, in all the reconstruction processes, a modified version of the 3D reconstruction algorithm (Penczek *et al*., 1992) was used with an enforced D_6 point-group symmetry.

Resolution. For the resolution limit estimation of 3D volumes, two subsets were randomly drawn and each subjected to a 3D reconstruction. The corresponding pairs of 3D volumes were then compared in reciprocal space on spherical shells with increasing radii using the differential phase residual (DPR) criterion with a phase residual threshold of 45° (Frank *et al*., 1981) and the Fourier shell correlation (FSC) criterion with a threshold coefficient of 0.5 (FSC is the 3D version of the Fourier ring correlation introduced by Saxton and Baumeister in 1982).

RESULTS

Monomer Content of HBL [T+L]. Band intensities of SDS−PAGE patterns, peak areas in HPLC elution chromatograms, and relative intensities of ESI-MS peaks were used to determine the monomer contents of native *Lumbricus* Hb and HBL[T+L]. All three methods showed that HBL-[T+L] contained 10.5 ± 0.5% of the monomer present in native Hb.

Cryoelectron Microscopy. Figure 1 shows a field of untilted-specimen images of native Hb examined in vitreous ice at a defocus of −2.7 μm. These images and their paired tilted-specimen images were recorded in view of the 3D reconstruction of volume V_A used as a reference in the refinements. Three main types of views are observed. In the first type, termed top view (black arrow), the molecule observed along its 6-fold axis of symmetry has a hexagonal contour. In the second type, called side view (white arrow), the rectangular contour indicates that the observation direction is perpendicular to the 6-fold axis. In addition, numerous intermediate views with ellipsoidal contours are present in the picture. Untilted-specimen images of native Hb and HBL[T+L] molecules were also recorded at a defocus of −1.5 μm for the refinements. They displayed less contrast and their shapes were difficult to recognize by eye. For these reasons they are not shown here.

3D Reconstruction. Because the purpose of this work was to compare the architectures of native Hb and HBL[T+L], the following strategy was used. First, a 3D volume of native Hb was calculated from tilted-specimen images taken at a relatively large defocus (−2.7 μm). Then, this volume was used as a reference for determining the Eulerian angles of the untilted-specimen images of both native and HBL[T+L] molecules observed at a smaller defocus (−1.5 μm).

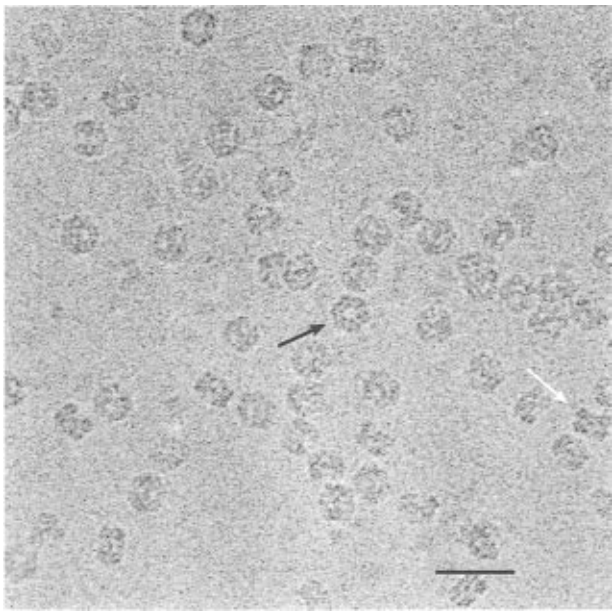

FIGURE 1: Untilted-specimen field of a frozen-hydrated sample of native *Lumbricus* Hb. Three types of EM views are observed: top view (black arrow), side view (white arrow), and intermediate views. The length of the scale bar is 65 nm.

Reconstruction of a Reference Volume of Native Hb. A series of 1416 pairs of tilted- and untilted-specimen single particle images of native Hb were interactively selected and windowed. After two-dimensional alignment, the untilted-specimen images were subjected to multivariate statistical analysis and automatic clustering to sort image classes which were homogeneous with respect to the specific orientations of the particles within the ice layer. A series of 32 homogeneous image classes was obtained from which four classes of top views (217 total images) and five classes of side views (175 total images) were selected and independently subjected to 3D reconstruction. The nine resulting primary volumes were aligned in a common orientation, and a merged 3D reconstruction volume was computed from the nine corresponding classes of tilted-specimen images (392 images). The merged 3D reconstruction volume was further refined by two cycles of 3D projection alignment and 3D reconstruction with an enforced D_6 point-group symmetry, thus producing the reference volume used at the next step. At this stage, the 1416 tilted-specimen images were included in the process and their Eulerian angles were determined by one cycle of 3D projection alignment.

In order to prevent deformation of the 3D reconstruction volume due to an oversampling of certain projection directions, a selection of the two images having the best correlation coefficients with the corresponding projection of the reference volume were selected for each projection direction. This procedure reduced the image set to 991 images and provided verification of the absence of important gap in the angular coverage. A new 3D reconstruction volume was calculated and three cycles of 3D projection alignment and iterative back projection produced three new

volumes. For each cycle, the reference was the volume calculated from the images with improved Eulerian angles and centration obtained at the previous cycle. The resolution of the final volume was estimated to 39.6 Å by the DPR criterion at a threshold of 45° and 35.6 Å by the FSC criterion at a correlation coefficient of 0.5 (a threshold that we estimate significant for this measure). The volume filtered down to the resolution limit of 35 Å is further termed V_A.

Refinement of the Volume of Native Hb by 3D Projection Alignment. The refinement of the 3D volume of native Hb was carried out on a set of 3421 images recorded at a defocus of −1.5 μm. Eulerian angles were assigned to all the images composing the image set by one cycle of 3D projection alignment using volume V_A as a reference. A selection of the best two images corresponding to each projection direction of the reference volume produced an image subset that was used to obtain a 3D reconstruction volume. This volume was submitted to three cycles of 3D projection alignment under the same conditions as for the native Hb. The resolution of the final volume was estimated to 27.6 and 26.2 Å by the DPR and FSC criteria, respectively. The volume was filtered down to 29.5 Å.

3D Reconstruction of the Reassembled HBL[T+L] Molecule. The method used for the refinement of the native Hb was also used to produce the 3D reconstruction volume of HBL[T+L] on a set of 2352 images recorded at a defocus of −1.5 μm. As above, Eulerian angles were assigned to all the images by one cycle of 3D projection alignment using volume V_A as a reference. A selection of the best two images corresponding to each projection direction of the reference volume produced an image subset that was used to obtain a 3D reconstruction volume. This volume was submitted to three cycles of 3D projection alignment under the same conditions as for the native Hb. The resolution of the final volume was estimated at 34.9 and 29.5 Å by the DPR and FSC criteria, respectively. The volume was filtered down to 29 Å.

Surface Representation of Native and HBL [T+L]: (1) Thresholding Method. Appearance of the reconstruction volume in the surface representation considerably depends on the threshold. The function of a threshold is to transform the distribution of the densities into a binary distribution by assigning values of 1 and 0 to protein and ice voxels, respectively. Thus, the higher the threshold, the more eroded is the aspect of the 3D volume. If one knows the molecular mass and the partial specific volume of the protein, the simplest method is to define the threshold as the value leading to the expected molecular volume. We used the molecular mass of 3.66 MDa and the partial specific volumes of the globin (0.738 $cm^3\ g^{-1}$) and linker (0.722 $cm^3\ g^{-1}$) chains determined by Martin *et al*. (1996b) to calculate the molecular volume of 4.46×10^6 $Å^3$ for native Hb on the basis of a 0.7:0.3 ratio of globin to linker chains. For calculation of the expected molecular volume of reassembled HBL[T+L], we assumed that the $3 \times 12 = 36$ copies of chain d were missing. Thus, using the weighted average molecular mass of chain d determined by ESI-MS by Martin *et al*. (1996b), a value of 3.084 MDa [$(3.66 \times 10^6) - (3 \times 12 \times 15\,983)$] was obtained. This gives a calculated molecular volume of 3.75×10^6 $Å^3$.

(2) The External Surfaces of Native Hb and HBL[T+L]. Figure 2 shows surface representations of native (A−C) and HBL[T+L] (D−F) reconstruction volumes corresponding to the expected molecular volume. The top views (Figure 2, panels A and D) show that both consist of two layers, each composed of six HGSs (open circles), with the vertices of the upper hexagonal layer 16° clockwise rotated relative to those of the lower layer. In this orientation, the distances between opposing vertices in native Hb and HBL[T+L] are 30.8 and 30.0 nm, respectively. Each HGS has a local 3-fold axis of symmetry (open triangle) that brings into coincidence the six constituent dense masses 1−6, observed at higher thresholds (Figure 5). In addition to the hexagonal central mass, only the masses 1−3 in each HGS and the c1 connections between masses 2 and 3 of neighboring HGSs are visible. The 45° views (Figure 2, panels B and E) show the six masses 1−6 in each HGS, the local 3-fold axis of symmetry (open triangle), and the c2 connections linking masses 4 and 6 of neighboring HGSs. The side views (Figure 2, panels C and F) show the interface between the hexagonal layers and the c4 connection area located around the 2-fold axis. In this orientation, the native Hb measures 28.8 nm in length and 20.2 nm in height and HBL[T+L] 27.8 nm in length and 20.0 nm in height.

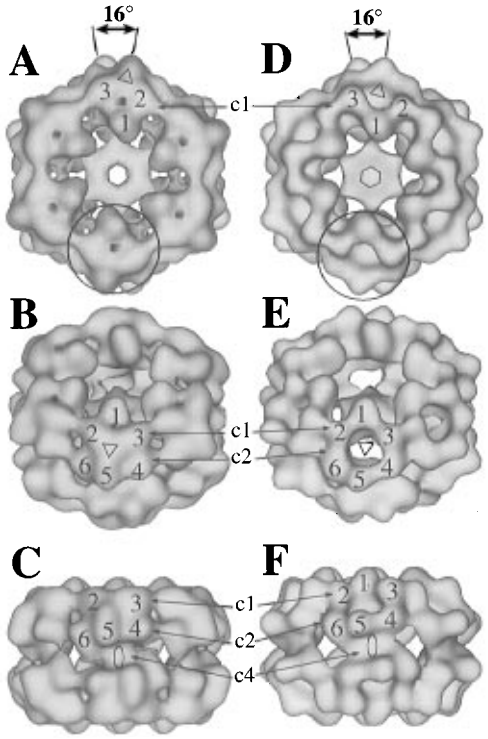

FIGURE 2: Surface representations at a threshold displaying the expected molecular volume of native (A−C) and HBL[T+L] (D−F) in the top view (A, D), the 45° view (B, E), and the side view (C, F). The 2-fold, 3-fold, and 6-fold axes are represented by the elliptic, triangular, and hexagonal, symbols. In panels A and D, notice that the vertices of the upper hexagonal half-molecules are 16° clockwise rotated around the 6-fold axis compared to those of the lower layer. Numbers 1−6 correspond to the HGS masses described in Figure 5. The open circle circumscribes one HGS. The c1, c2, and c4 symbols refer to the connections described in the text.

(3) Surface Representation of the Internal Structure. Figures 3 and 4 show sections of the Hb and HBL[T+L] volumes cut perpendicular to and along the 6-fold axis, respectively. The two sections in Figure 3 show that the floor of each HGS consists of masses 4−6 and that there is an internal bracelet of connections, termed c3, linking masses 4 and 6 in all the HGSs within each layer (Figure 3, panels

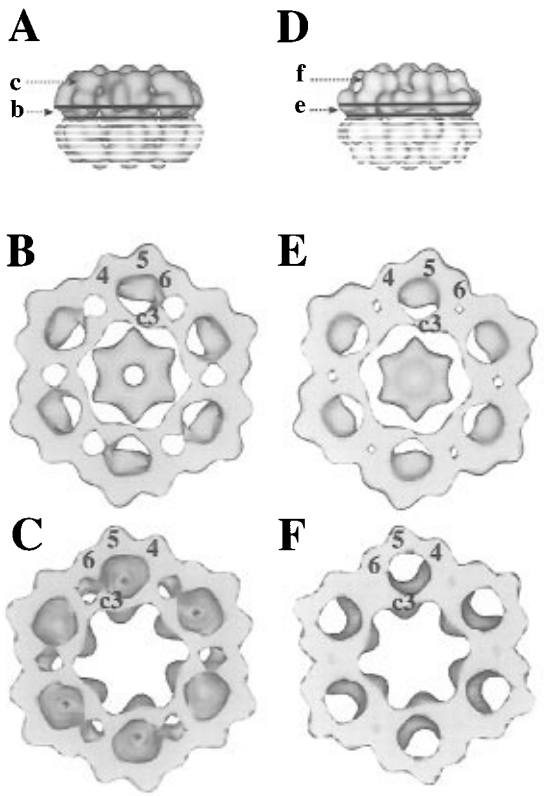

FIGURE 3: Solid-body surface representation of the 3D reconstruction volume of native Hb and HBL[T+L] cut perpendicularly to the 6-fold axis and displayed at a threshold displaying the expected molecular volume. The central (B, E) and upper (C, F) fragments are obtained by cutting the whole volume as represented by the black lines in panels A and D. The central fragment is viewed from the top to show the floor of the HGSs. The upper fragment is viewed from below to show the ceiling of the HGSs. Numbers 1−6 correspond to the HGS masses described in Figure 5.

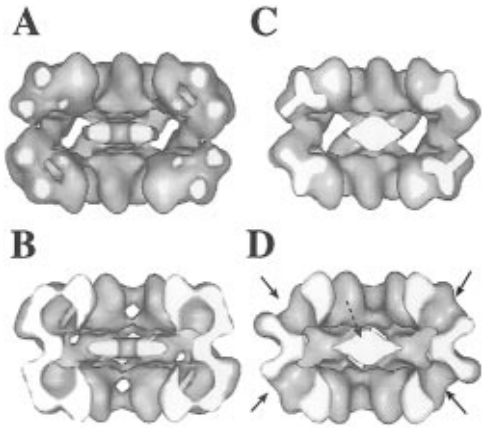

FIGURE 4: Solid-body surface representation at a threshold displaying the expected molecular volume of the 3D reconstruction volumes of native Hb (A, B) and HBL[T+L] (C, D) cut by planes passing by the 6-fold axis and perpendicular to one of the 2-fold axes. The cutting plane passes between neighboring HGSs (A, C) and through HGSs (B, D). Notice that the thin c5 connections are not visible at this threshold. Black arrows in panel D show the missing material visible in panel B. The dashed arrow in panel D points to the ellipsoidal shape of the central mass to be compared to the toroid in panel B.

B and E). The sections shown in Figure 3, panels C and F, demonstrate that while the ceiling of each HGS cavity in native Hb is completely closed, each HGS in HBL[T+L] has a large central hole, about 4 nm in diameter. Figure 4 shows the Hb and HBL[T+L] volumes cut in halves by

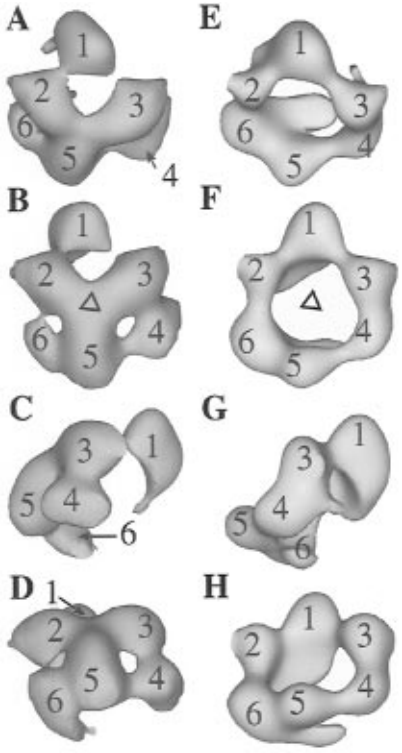

FIGURE 5: The structure of the HGS in native *Lumbricus* Hb (A−D) and HBL[T+L] (E−H) observed at a threshold displaying 17% of the expected molecular volume. (A, E) Top views observed along the HBL 6-fold axis; (B, F) 45° views with the local pseudo 3-fold axis oriented toward the observer. (C, G) Lateral views. (D, H) Side views seen along one 2-fold axis. The numbers mark the location of the six high-density masses.

planes containing the 6-fold axis and passing between (Figure 4, panels A and C) and through (Figure 4, panels B and D) the HGSs. The appearance of the half-molecule cut between the HGSs in both the Hb and HBL[T+L] (Figure 4, panels A and C) are almost identical. The HBL[T+L] (Figure 4, panels C and D) differs from Hb (Figure 4, panels A and B) by the loss of material located around the local 3-fold axis in the external part of the HGS wall and ceiling (four arrows in Figure 4D) and in having an ellipsoidal central mass (dashed arrow in Figure 4D) instead of a toroid structure.

The HGS Architecture Observed at High Threshold. Figure 5 shows single HGSs extracted from the 3D reconstruction volumes of Hb and HBL[T+L] by careful masking of the neighboring structures at a threshold leaving apparent 17% of the expected molecular volume. Each HGS contains six masses, which are designated 1−6. The top view orientations (Figure 5, panels A and E) show clearly that despite the missing material in HBL[T+L] there are six masses closely correspondent to those in the Hb. In the 45° view (Figure 5, panels B and F), the material missing in HBL[T+L] is symmetrically disposed around the local 3-fold axis. The examination of the lateral (Figure 5, panels C and G) and side (Figure 5, panels D and H) views confirms this conclusion. However, the disposition and size of the six masses are not perfectly similar: in HBL[T+L], masses 2 and 6 are connected to each other (Figure 5, panels F and H) and mass 1 appears larger than in the native Hb (Figure 5, panels C and G).

The Internal Organization of the Native and HBL[T+L] Molecules. Although the differences shown in Figures 2−5 are clear, they are based on surface representations that are

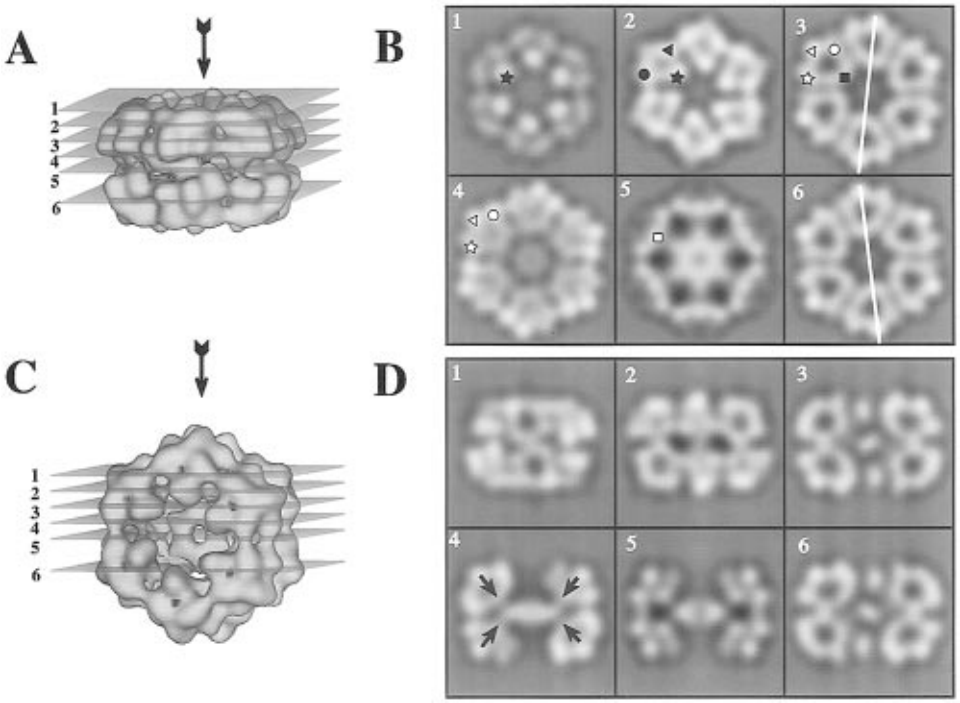

FIGURE 6: Shaded surface representation and sections through the reconstructed volume of native *Lumbricus* Hb. (A) Levels of the sections perpendicular to the 6-fold axis shown in panel B. (C) Levels of the sections perpendicular to the 2-fold axis shown in panel D. The thickness of each section is 1 voxel, i. e., 7.37 Å. In panels A and B, the black arrows show the observation direction. The HGS masses are symbolized by closed star (mass 1), closed triangle (mass 2), closed circle (mass 3), open star (mass 4), open triangle (mass 5), and open circle (mass 6). In panels B3 and B6, the white bars allow comparison of respective orientations of the two hexagonal layers. In panel D4 the black arrows point to the c5 connections.

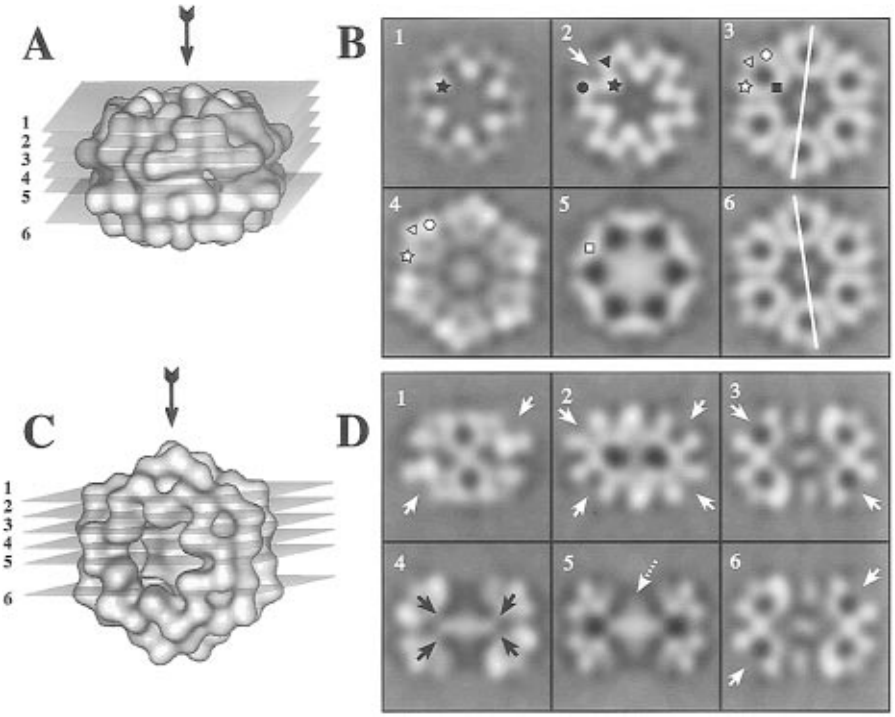

FIGURE 7: Shaded surface representation and sections through the reconstructed volume of native and reassociated HBL[T+L]. (A) Levels of the sections perpendicular to the 6-fold axis shown in panel B. (C) Levels of the sections perpendicular to the 2-fold axis shown in panel D. The thickness of each section is 1 voxel, i.e., 7.26 Å. In panels A and B, the black arrows show the observation direction. The HGS masses are symbolized by closed star (mass 1), closed triangle (mass 2), closed circle (mass 3), open star (mass 4), open triangle (mass 5), and open circle (mass 6). In panels B3 and B6, the white bars allow comparison of respective orientations of the two hexagonal layers. The white arrows point to the presumed location of the missing chain d. In panel D4, the black arrows point to the c5 connections. In panel D5, the dashed white arrow shows the domed-up structure of the central mass.

themselves dependent on the threshold value. One efficient way to check the results is to examine the optical densities of thin slices through the 3D volumes. Figures 6 and 7 show selected 1 voxel thick slices perpendicular to the 6-fold and 2-fold axes through the 3D volumes of native Hb and HBL-[T+L], respectively. As shown in the first slices (Figures

6B1 and 7B1) six high-density areas closest to the 6-fold axis correspond to the six HGS masses 1 (closed star). In the second slices (Figures 6B2 and 7B2), these same masses and 12 additional masses with more external locations are visible in both molecules. Masses located on the right and left sides of each HGS, when seen from the 6-fold axis, corresponds to mass 2 (closed triangle) and 3 (closed circle), respectively. However, the contour of the particle looks completely different in the two molecules because of the absence in HBL[T+L] of the material located close to the hexagon vertices (white arrow). The next two slices (Figures 6 and 7, panels B3 and B4) show the bottom of the upper layer HGS cavity which is very similar in the two molecules. In Figures 6B3 and 7B3, masses 4 (open star), 5 (open triangle), and 6 (open circle) appear as densities located on the HGS external wall and the c3 connection bodies of the six HGSs form an inner wall boarding the large hexagonal central opening of the HBL (closed square). Masses 4−6 are also visible in Figures 6B4 and 7B4 as high-density nuclei in the external HGS wall. The fifth slices (Figures 6B5 and 7B5) show the central hexagonal mass and the six c4 connection bodies (open square) linking the two hexagonal layers cut transversely. The sixth slices (Figures 6B6 and 7B6) are similar to each other and enantiomorphic to the third slices (Figures 6B3 and 7B3). The reason for this phenomenon lies in the position of the 2-fold symmetry axes, which are not superposed to the lines joining opposed vertices in the hexagonal layer.

Slices perpendicular to the 2-fold axes are also useful for understanding the internal architecture and differences between native Hb and HBL[T+L]. The first slices (Figures 6D1 and 7D1) are almost perfectly identical except for a notch in the upper right and lower left areas (arrows). This corresponds to the material missing in the upper part of the HGS (Figure 7D1). This absence of material is also very clear in slices D2, D3, and D6 (arrows) in Figure 7. The second difference between native and HBL[T+L] is the domed shape of the central hexagonal mass in the latter molecule. This is obvious from the comparison of Figures 6D5 and 7D5 (dashed arrow). In addition, Figures 6D4 and 7D4 provide the opportunity to observe the two c5 connections (black arrows) linking each vertex of the central hexagonal mass (appearing here as central horizontal mass) to the c3 connection body of the upper and lower HGS layers. These c5 connections were not visible in the surface representations of Figure 2 at the threshold displaying the expected molecular volume, but they are visible at higher thresholds.

DISCUSSION

The D_6 point-group symmetry observed for *Lumbricus* Hb crystals (Royer *et al*., 1987; Royer & Hendrickson, 1988) and 3D reconstructions from EM images of two-dimensional crystals of *Eophila* and *Ophelia* Hbs (Cejka *et al*., 1989, 1991, 1992) has been verified by the cryoelectron microscopic 3D reconstruction of *Lumbricus* Hb (Schatz *et al*., 1995), *Eudistylia* Chl (De Haas *et al*., 1996b), *Macrobdella* Hb (De Haas *et al*., 1996a), the deep sea Hbs from *Riftia* (De Haas *et al*., 1996c), and *Alvinella* (De Haas *et al*., 1996d) and now of *Lumbricus* Hb and its reassembled form HBL-[T+L]. Furthermore, all the 3D reconstructions determined by cryoelectron microscopy, including the ones obtained in the present study, also demonstrate the presence of a very important feature of the quaternary structure of HBL Hbs, namely the existence of a local 3-fold symmetry in each of the 12 HGSs forming the two layers. This local 3-fold symmetry is consonant with the top portion of each HGS corresponding to a dodecamer of globin chains $[a + b + c]_3[d]_3$ and is in agreement with the local 3-fold symmetry found in the crystal structure of the isolated *Lumbricus* Hb dodecamer subunit (Martin *et al*., 1996a). It should be emphasized that such a local 3-fold symmetry is incompatible with the HGS consisting of a hexadecamer of globin chains $[a + b + c]_4[d]4_4$ as proposed by Riggs *et al*. (Ownby et al., 1993, Zhu *et al*., 1996a,b). The other general and unexpected feature of the HBL quaternary structure appears to be the ∼16° clockwise rotation of the vertices of the upper hexagonal layer relative to those of the lower ones, observed by us in all cases except the Hb from the deep sea annelid *Alvinella* (De Haas *et al*., 1996d), where both layers were in the eclipsed conformation. Unlike the 3D reconstruction of *Lumbricus* Hb by Schatz *et al*. (1995), which used the angular reconstitution method based on untilted-specimen images, our 3D reconstructions use the random conical tilt series method and tilted-specimen images and thus provide structures with absolute chirality. A puzzling aspect of the observed staggered conformation of the two layers in the HBL quaternary structure is that the rotation is only about half the 30° expected of a fully staggered conformation.

It should be noted that the state of oxygenation of the HBL Hbs in the vitreous ice during the collection of the transmission EM image is unknown. Although the specimens are prepared using the oxy form, it is possible that, during the fall into the cryogen, the exposure of the liquid specimen to a nitrogen-rich gas phase may induce a loss of oxygen accompanied by conversion to the deoxy form. However, the wide variation in the P_{50}, from >100 torr for *Eudistylia* Chl (Imai *et al*., 1996), ∼12 torr for *Lumbricus* Hb (Fushitani *et al*., 1986; Vinogradov *et al*., 1991), ∼5 torr for *Macrobdella* Hb (Weber *et al*., 1995), and ∼0.3 torr for *Riftia* and *Alvinella* Hbs (Arp *et al*., 1990; Toulmond *et al*., 1990), suggests that partial oxy to deoxy conversion is unlikely to be responsible for the observed rotation of the two layers. Clearly, the state of ligation of the HBL Hbs during the course of cryoEM measurements merits further investigation. Until more light is shed on this matter, we would like to suggest that relative rotation of the two hexagonal layers around the 6-fold axis could play a role in the mechanism underlying the enhanced cooperativity of oxygen binding of the HBL Hbs relative to the cooperativity of the isolated functional globin subunits (Lamy *et al*., 1996). The latter are a 213 kDa dodecamer in *Lumbricus* Hb, a 65 kDa tetramer in *Macrobdella* Hb, and a dodecamer in *Eudistylia* Chl (Vinogradov *et al*., 1991; Kapp *et al*., 1990; Qabar *et al*., 1991). Although the oxygen binding affinities of these subunits are either similar to the native Hb as in *Lumbricus* (Vinogradov *et al*., 1991) or higher, as in *Macrobdella* Hb (Weber *et al*., 1995) and *Eudistylia* Chl (Imai *et al*., 1996), their cooperativities as expressed by the Hill coefficient at half-saturation n_{50} are in the range 1.4−2.1, considerably smaller than those of the native molecules n_{50} ∼3−4. These results suggest that the overall cooperativity of oxygen binding of the HBL Hbs may consist of two components, one due to globin−globin interactions within the subunits and the other due to linker-mediated globin−subunit interactions. It is the latter that we think may be related to the

observed partial rotation of the two layers. Recent small angle X-ray scattering studies of *Lumbricus* Hb and dodecamer have shown the absence of detectable alteration in their molecular shapes in going from oxy to deoxy and back (Krebs *et al*., 1996a,b), in agreement with the likely absence of detectable alteration in molecular shape resulting from any relative rotation of the two layers.

All the 3D reconstructions obtained by the conical tilt series method display several additional common features. (i) Each HGS can be resolved into six dense masses 1−6 by progressively raising the threshold density used to represent the volume. (ii) There are connections c1 and c2 between masses 3 and 4 of one HGS with masses 2 and 6, respectively, of the two neighboring HGSs. (iii) A central linker complex is always present, consisting of a central flat hexagonal mass linked through 12 c5 connections to two bracelets of c3 connections and one set of six c4 connections to masses 4 and 6 of each HGS. These details are easily seen in the 3D reconstructions of *Lumbricus* Hb and its reassembled HBL[T+L] shown in Figures 2 and 3.

The most remarkable result evident from a comparison of the two 3D reconstructions (Figures 2−4) is the overwhelming similarity of their respective architectures when examined in the most exacting detail at the ∼35 Å resolution obtained in this work. One main difference is the absence of material located around the local 3-fold axis of each HGS in HBL-[T+L], so that the 3D volume of each HGS has large central cavities in the top (Figure 2D), side (Figure 2F), and 45° (Figure 2E) views and appears perforated in the upper fragment view (Figure 3F) and in the cross-section view (Figure 4D). The only other differences, both minor and unexplained, are the increased thickness of the central mass (Figure 4, panels C and D) and the slight increase in mass 1 of each HGS in the HBL[T+L] (Figure 5, panels C and G). Comparison of the two structures determines the locus of the three monomer subunits (chain d) in the dodecamer complex and illustrates the potential usefulness of our approach.

Kapp *et al*. (1987) examined the negatively stained, summed and averaged images of the Hb and HBL[T+L] using STEM and found the reassembled HBL to be smaller, with a vertex to vertex diameter of 25.0 nm versus 30.7 nm. A simple subtraction of the two images, followed by rescaling to remove negative pixel values and expanding the grey scale to 8-bit precision, resulted in a hexagonal, peripheral ring of stain density, suggesting that the location of the monomer subunit was at the periphery of the HBL structure. Although at first glance, this result appears to contradict our finding, a simple simulation of negative staining of native Hb and HBL[T+L], followed by the calculation of a subtraction volume and a projection of this volume, produces images shown in Figure 8, which are similar to those of Kapp *et al*. (1987). Our simulation experiment explains the peripheral distribution of the difference in the subtraction images. Indeed, since in HBL-[T+L] the empty cavity resulting from the absence of monomer subunits within each HGS can accommodate more stain than in native Hb and since scaling of the stain intensities in this region in the Hb and the HBL[T+L] images are approximately the same, as was done by Kapp *et al*. (1987), then the stain intensity at the periphery of the HBL-[T+L] relative to the Hb is reduced.

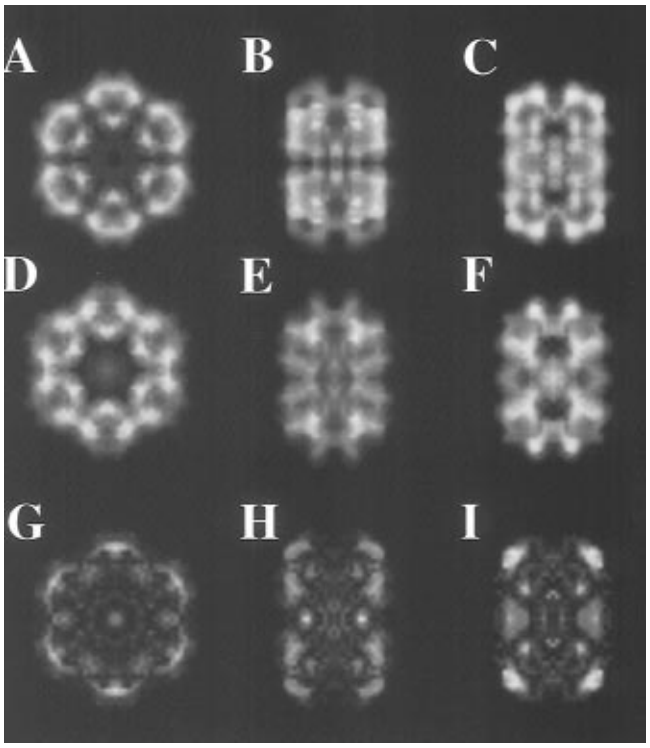

FIGURE 8: Simulation of double carbon layer negative staining of native (A−C) and reassociated HBL[T+L] (D−F) and subtraction image (G−I) between the two volumes. The 3D reconstruction volumes oriented in their top (A, D), side 1 (B, E), and side 2 (C, F) views were thresholded so that the expected molecular volume is enclosed in the surface representation. Then, densities of 0 (black in the figure) and 1 (white in the figure) were assigned to all voxels located outside and inside the molecular surface, respectively. Finally, densities were projected and summed along the 6-fold and 2-fold symmetry axes. The difference projection images (G−I) result from a subtraction of the HBL[T+L] from the native volume followed by a rescaling to remove the negative values.

All the 3D reconstructions taken together provide a firm basis for the "bracelet" model of HBL Hb structure, originally proposed for *Lumbricus* Hb (Vinogradov *et al*., 1986), consisting of 12 dodecamers of globin chains decorating a bracelet of 36−42 linker chains. Recent ESI-MS studies of subunit and polypeptide chain compositions of the HBL Hbs from *Tylorrhynchus* (Green *et al*., 1995), *Macrobdella* (Weber *et al*., 1995), *Riftia* (Zal *et al*., 1996a), and *Arenicola* (Zal *et al*., 1996b) have demonstrated that this model is applicable to them as well.

ACKNOWLEDGMENT

We thank Brian N. Green for performing the ESI-MS analyses of the native Hb and HBL[T+L] and Drs. Mona Norcum and Nicolas Boisset for their help in correcting the manuscript.

REFERENCES

Adrian, M., Dubochet, J., Lepault, J., & McDowall, A. W. (1984) *Nature 308*, 32−36.

Arp, A. J., Doyle, M. L., Di Cera, E., & Gill, S. J. (1990) *Resp. Physiol. 80*, 323−334.

Boekema, E. J., & Van Heel, M. (1989) *Biochim. Biophys. Acta 957*, 370−379.

Boisset, N., Penczek, P., Pochon, F., Frank, J., & Lamy, J. N. (1993) *J. Mol. Biol. 232*, 522−529.

Cejka, Z., Ghiretti-Magaldi, A., Tognon, G., Zanotti, G., & Baumeister, W. (1989) *J. Ultrastruct. Mol. Struct. Res. 102*, 71−81.

Cejka, Z., Santini, C., Tognon, G., & Ghiretti-Magaldi, A. (1991) *J. Struct. Biol. 107*, 259−267.
Cejka, Z., Kleinz, J., Santini, C., Hegerl, R., & Ghiretti-Magaldi, A. (1992) *J. Struct. Biol. 109*, 52−62.
De Haas, F., Boisset, N., Taveau, J. C., Lambert, O., Vinogradov, S. N., & Lamy, J. N. (1996a) *Biophys. J. 70*, 1973−1984.
De Haas, F., Taveau, J.-C., Boisset, N., Lambert, O., Vinogradov, S. N., & Lamy, J. N. (1996b) *J. Mol. Biol. 255*, 140−163.
De Haas F., Zal, F., Lallier, F. H., Toulmond, A., & Lamy, J. N. (1996c) *Proteins 26*, 241−256.
De Haas, F., Zal, F., You, V., Lallier, F., Toulmond, A., & Lamy, J. N. (1996d) *J. Mol. Biol. 264*, 111−120.
Dubochet, J., Lepault, J., Freeman, R., Berriman, J. A., & Homo, J. C. (1982) *J. Microsc. 128*, 219−237.
Frank, J., Verschoor, A., & Boublik, M. (1981) *Science 214*, 1353−1355.
Frank, J., Radermacher, M., Penczek, P., Zhu, J., Li, Y., Ladjadj, M., & Leith, A. (1996) *J. Struct. Biol. 116*, 190−199.
Fushitani, K., Imai, K., & Riggs, A. F. (1986) *J. Biol. Chem. 261*, 8414−8423.
Gilbert P. F. C. (1972) *Proc. R. Soc. London, Ser. B 182*, 89−117.
Green, B. N., Suzuki ,T., Gotoh, T., Kuchumov, A. R., & Vinogradov, S. N. (1995) *J. Biol. Chem. 270*, 18209−18211.
Harauz, G., & Ottensmeyer, F. P. (1984) *Ultramicroscopy 12*, 309−320.
Imai, K., Sharma, P. K., & Vinogradov, S. N. (1996) *Comp. Biochem. Physiol. 113B*, 613−618.
Kapp, O. H., Polidori, G., Mainwaring, M. G., Crewe A. V., & Vinogradov, S. N. (1984) *J. Biol. Chem. 259*, 628−639.
Kapp, O. H., Mainwaring, M. G., Vinogradov, S. N., & Crewe, A. V. (1987) *Proc. Natl. Acad. Sci. U.S.A. 84*, 7532−7536.
Kapp, O. H., Qabar, A. N., Bonner, M. C., Stern, M. S., Walz, D. A., Schmuck, M., Pilz, I., Wall, J. S., & Vinogradov S. N. (1990) *J. Mol. Biol. 213*, 141−158.
Krebs, A., Kuchumov, A., Sharma, P. K., Braswell, E. H., Zipper, P., Weber, R. E., & Vinogradov, S. N. (1996a) *J. Biol. Chem. 271*, 18695−18704.
Krebs, A., Zipper, P., & Vinogradov, S. N. (1996b) *Biochim. Biophys. Acta 1297*, 115−118.
Laemmli, U. (1970) *Nature 227*, 680−685.
Lambert, O., Boisset, N., Taveau, J. C., Préaux, G., & Lamy, J. N. (1995) *J. Mol. Biol. 248*, 431−448.
Lamy, J. N., Green, B. N., Toulmond, A., Walls, J. S., Weber, R. E., & Vinogradov, S. N. (1996) *Chem. Rev. 96*, 3113−3124.
Lebart, L., Morineau, A., & Warwick, K. M. (1984) *Multivariate Descriptive Statistical Analysis*, pp 117−143, Wiley, J., & Sons, New York.
Martin, P. D., Eisele, K. L., Doyle, M. A., Kuchumov, A. R., Walz, D. A., Arutyunyan, E. G., Vinogradov, S. N., & Edwards, B. F. P. (1996a) *J. Mol. Biol. 255*, 170−175.
Martin, P. D., Kuchumov, A. R., Green, B. N., Oliver, R. W. A., Braswell, E. H., Wall, J. S., & Vinogradov S. N. (1996b) *J. Mol. Biol. 255*, 154−169.
Milligan, R. A., Brisson, A., & Unwin, P. N. T. (1984) *Ultramicroscopy 13*, 1−10.
Misell, D. L. (1978) in *Practical Methods in Electron Microscopy* (Glauert, A. M., Ed.) Vol. 7, pp 33−90, North-Holland, Amsterdam.
Ownby, D. W., Zhu, H., Schneider, K., Beavis, R. C., Chait, B. T., & Riggs, A. F. (1993) *J. Biol. Chem. 268*, 13539−13547.
Penczek, P., Radermacher, M., & Frank, J. (1992) *Ultramicroscopy 40*, 33−53.
Penczek, P., Grassucci, R., & Frank, J. (1994) *Ultramicroscopy 53*, 251−270.
Qabar, A. N., Stern, M. S., Walz, D. A., Chiu, J. T., Timkovich, R., Wall, J. S., Kapp, O. H., & Vinogradov, S. N. (1991) *J. Mol. Biol. 222*, 1109−1129.
Radermacher, M. (1988) *J. Electron. Microsc. Tech. 9*, 359−394.
Radermacher, M., Wagenknecht, T., Verschoor, A., & Frank, J. (1987a) *EMBO J. 6*, 1107−1114.
Radermacher, M., Wagenknecht, T., Verschoor, A., & Frank, J. (1987b) *J. Microsc. 146*, 113−136.
Royer, W. E., Jr, & Hendrickson, W. A. (1988) *J. Biol. Chem. 263*, 13762−13765.
Royer, W. E., Jr, Hendrickson, W. A., & Love, W. E. (1987) *J. Mol. Biol. 197*, 149−153.
Saxton, W. O., & Baumeister, W. (1982) *J. Microsc. 127*, 127−128.
Schatz, M., Orlova, E. V., Dube, P., Jäger, J., & Van Heel, M. (1995) *J. Struct. Biol. 114*, 28−40.
Sharma, P. K., Kuchumov, A., Chottard, G., Martin, P. D., Wall, J. S., & Vinogradov, S. N. (1996), *J. Biol. Chem. 271*, 8754−8762.
Taveau, J. C. (1996) *J. Struct. Biol. 116*, 223−229.
Toulmond, A., El-Idrissi Slitine, F., De Frescheville, J., & Jouin, C. (1990) *Biol. Bull. 179*, 366−373.
Van Heel, M. (1984) *Ultramicroscopy 13*, 165−184.
Van Heel, M., & Frank, J. (1981) *Ultramicroscopy 6*, 187−194.
Vinogradov, S. N., & Sharma, P. K. (1994) *Methods Enzymol. 231*, 112−124.
Vinogradov, S. N., Lugo, S. D., Mainwaring, M. G., Kapp, O. H., & Crewe, A. V. (1986) *Proc. Natl. Acad. Sci. U.S.A. 83*, 8034−8038.
Vinogradov, S. N., Sharma, P. K., Qabar, A. N., Wall, J. S., Westrick, J. A., Simmons, J. H., & Gill S. J. (1991) *J. Biol. Chem. 266*, 13091−13096.
Ward, J. H. (1963) *J. Am. Stat. Assoc. 58*, 236−244.
Weber, R. E., Malte, H., Braswell, E. H., Oliver, R. W. A., Green, B. N., Sharma, P. K., Kuchumov, A., & Vinogradov, S. N. (1995) *J. Mol. Biol. 251*, 703−720.
Zal, F., Green, B. N., Lallier, F., Vinogradov, S. N., & Toulmond, A. (1996a) *J. Biol Chem. 271*, 8875−8881.
Zal, F., Green, B. N., Lallier, F., Vinogradov, S. N., & Toulmond, A. (1997) *Eur. J. Biochem. 243*, 85−92.
Zhu, H., Hargrove, M., Xie, Q., Nozaki, Y., Linse, K., Smith, S. S., Olson, J. S., & Riggs, A. F. (1996a) *J. Biol. Chem. 271*, 29999−30006.
Zhu, H., Ownby, D. W., Riggs, C. K., Nolasco, N. J., Stoops, J. K., & Riggs, A. F. (1996b) *J. Biol. Chem. 271*, 30007−30021.

BI970131L